Proceedings of the 19th International Symposium on the
Packaging and Transportation of Radioactive Materials
PATRAM 2019
August 4-9, 2019, New Orleans, LA, USA

Temperature Prediction of a TN-32 Cask with Non-Concentric Basket Subjected to Vacuum Drying

Megan Higley, Mustafa Hadj-Nacer, and Miles Greiner
Department of Mechanical Engineering, University of Nevada, Reno, NV, USA

Abstract

In this work, geometrically-accurate two-dimensional computational fluid dynamic models of a used nuclear fuel cask that can contain up to 32 pressurized water reactor (PWR) fuel assemblies are constructed. These models are similar to the TN-32 cask currently employed in the ongoing high-burnup (HBU) Spent Fuel Data Project lead by the Electric Power Research Institute (EPRI). These models are used to predict the peak cladding temperature (PCT) under vacuum drying conditions.

In a typical TN-32 cask, the fuel basket is designed to be concentric inside the cask, leaving a constant 4.8-mm gap with the aluminum rails. Previous work by the authors showed that this gap accounts for a significant increase in the PCT. In this work, we will investigate the effect of the fuel basket leaning on one or two sides of the cask, closing the gap on those sides, and enlarging it on the opposite sides. Steady-state simulations that include the temperature-jump boundary conditions at the gas-solid interfaces to into account the rarefaction effect at low pressures will be performed for a range of dry helium pressures ranging from ~10^5 to 100 Pa in all the configurations (concentric, single-side leaning, and double-side leaning). The PCT will be reported for different pressures. The maximum allowable heat generation that brings the cladding temperatures to the radial hydride formation limit of 400°C will be also reported.

Introduction

Used nuclear fuel (UNF) assemblies are stored in water pools to reduce their radioactivity and heat generation rates [1]. After a few years in the pool, a cask with an internal basket is lowered into the pool and loaded with the fuel assemblies. It is then sealed, lifted out of the pool and drained [2]. A small amount of water may remain at the bottom or in crevices of the cask, and on the cladding surfaces after draining. All the remaining moisture must be removed before the cask is filled with helium (or nitrogen) and transported to a long-term storage facility to avoid any corrosion of internal components or formation of a combustible mixture of hydrogen and oxygen [3]. Vacuum drying is widely used to remove moisture from the fuel casks before placing them for long-term storage [4]. During this process, the pressure is reduced to as low as 67 Pa to promote evaporation and removal of water [4]. The process continues until the cask can hold a pressure of less than 400 Pa for at least 30 minutes as specified by the Nuclear Regulatory Commission (NRC) Interim Staff Guidance-11, Revision 3 (ISG-11) [5]. NRC ISG11 [5] also requires that the

temperature of the fuel cladding must remain below roughly 400°C for normal conditions of loading and storage to avoid the formation of radial hydrides with the cladding that might affect their ductility and make them brittle and unsuitable for transportation.

The fuel cladding may experience their highest temperature during vacuum drying because it is the first operation they are removed from water to helium environment, which has relatively lower thermal conductivity, while their heat generation is still relatively high. In addition, the low-pressure conditions during vacuum drying may cause the temperature in the cask to further increase due to the rarefaction effect, which causes an additional thermal resistance (also called "temperature-jump") at the gas-solid interfaces [6].

Previous work by the authors [7] showed that the gap between the basket and rails accounts for most of the temperature increase due to the rarefaction effect (temperature-jump). In this work, the effect of the basket leaning on one or two sides of the cask, causing the gap to close on those sides and enlarge on the opposite sides is investigated. Geometrically-accurate two-dimensional (2D) computational fluid dynamic (CFD) models of a used nuclear fuel cask that can contain up to 32 pressurized water reactor (PWR) fuel assemblies are constructed. These models are similar to the TN-32 cask [8, 9] currently employed in the ongoing high-burnup (HBU) Spent Fuel Data Project lead by the Electric Power Research Institute (EPRI) [10]. Steady-state CFD simulations that include the temperature-jump boundary conditions at the gas-solid interfaces are performed for a range of dry helium pressures ranging from ~10^5 to 100 Pa in all the configurations (concentric, single-side leaning, and double-side leaning). Results are reported in term of peak cladding temperature (PCT) and maximum allowable heat generation rate that causes the PCT to reach the limit of radial hydride formation, T_{RH} = 400°C.

Heat Transfer through Rarefied Gas

At high pressures, the number of collisions between molecules and the walls is large enough to assume continuity of macroscopic properties, such as temperature, velocity, and partial pressure at the gas-solid interfaces. However, at low pressures, there are fewer collisions between gas molecules and the wall that causes a discontinuity of these macroscopic properties at the interfaces. The Knudsen number,

$$Kn = \frac{\lambda}{L_C}, \tag{1}$$

is the ratio of the mean free path of a molecule, λ, to a characteristic length, L_C, of a system. The characteristic length is usually the smallest dimension in the system. The mean free path is the average distance molecules will travel between successive collisions and is given by

$$\lambda = \frac{\mu}{P}\sqrt{2\frac{k_B}{m}T}, \tag{2}$$

where P is the pressure, T is the temperature, k_B is Boltzmann's constant, m is the molecular mass of the gas, and μ is the dynamic viscosity. The Knudsen number can be used for the classification of the rarefaction regimes [11]; (i) For $Kn \leq 10^{-3}$, the gas is in the *continuum* regime, where flow and heat transfer can be modeled using the Convective Energy and Navier-Stokes equations. (ii)

For $Kn \in [10^{-3}, 10^{-1}]$, the gas is in the *slip* regime, where the Convective Energy and Navier-Stokes equations are still valid, given that the slip boundary conditions of temperature, velocity and partial pressure are applied at the gas-solid interfaces. (iii) For $Kn \in [10^{-1}, 10]$, the gas is in the *transitional* regime, where the continuum approximation breaks down and the collisional Boltzmann equation should be used to model the gas. (iv) For Kn >10, the gas is in the *free molecular* regime, where the collisionless Boltzmann equation can be employed to model the gas because the interaction between gas molecules is negligible.

Given the dimensions of the UNF casks and the pressures during vacuum drying, helium is in the slip regime. In this regime, there is a temperature-jump that develops at the gas-solid interfaces and has to be taken into account to accurately model heat transfer. This temperature-jump acts as a resistance to heat transfer by conduction and can be described as

$$T_g - T_w = \zeta_t \lambda \left.\frac{\partial T}{\partial y}\right|_w , \tag{3}$$

where T_g is the temperature of the gas at the interface with the wall, T_w is the temperature of the wall, y is the coordinate normal to the wall, and ζ_T is the temperature-jump coefficient. Several temperature-jump models have been proposed in the literature. In this work, we will use the Lin & Willis model [6], as it was shown in a previous work [7] that this model accurately predict the temperature-jump in the slip regime. This model gives

$$\zeta_T = \left(\frac{2-\alpha}{\alpha} + 0.17\right)\frac{\gamma\sqrt{\pi}}{(\gamma+1)Pr}, \tag{4}$$

where γ is the ratio of specific heats at constant pressure and Pr is the Prandtl number (for helium γ =5/3 and Pr = 2/3). The parameter α in Eq. 4 is the thermal accommodation coefficient (TAC) that characterize how much energy a molecule exchange with the wall that interacts with it. Using the incident, T_i, and reflected, T_r, temperatures of a molecule, α can be expressed as

$$\alpha = \frac{T_i - T_r}{T_i - T_w}. \tag{5}$$

The values of α range from 0 to 1, with α=0 corresponding to a specular reflection (no energy exchange between the molecule and wall, $T_r = T_i$), and α=1 corresponding to a diffuse reflection (the molecule accommodates the wall temperature, $T_r = T_w$). Typical values of α for helium on a stainless steel surface found in the literature are in the range of 0.4 to 0.2 for a temperature between 10°C to 495°C, respectively [12]. For helium on a zircaloy surface, α = 0.34 was reported for a temperature of 25°C [13].

Numerical Models

A geometrically-accurate 2D model of a UNF cask designed to contain up to 32 Westinghouse 17x17 PWR assemblies is created and meshed in the ANSYS package. Figure 1 shows the material details of this model with a zoom showing portions of the fuel rods, channels, basket, rails, vessels, and the 4.78-mm gap between the rails and basket. This gap is of particular interest for this work and will be discussed further below.

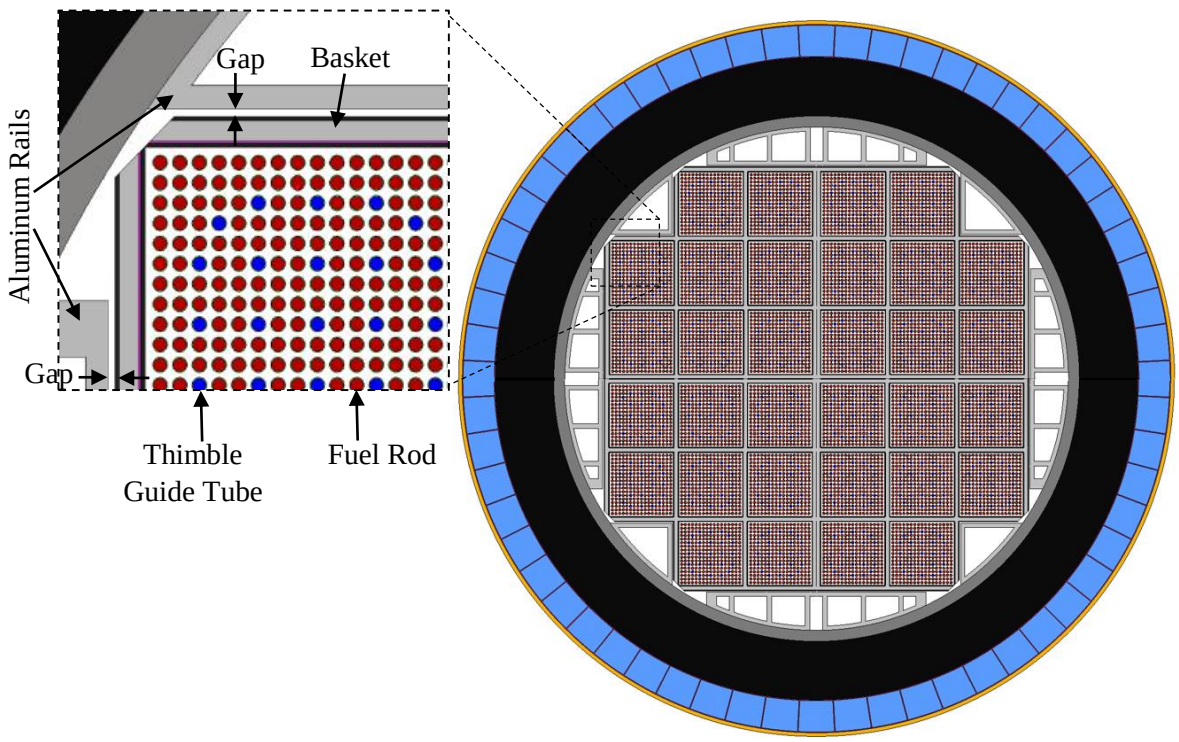

Figure 1: Material details of the geometrically-accurate 2D model with a zoom showing a region of the fuel rod array, channels, basket grid, aluminum rails, and vessels. The 4.78 mm gap between the basket and aluminum rails is highlighted.

The diameter of the fuel rods is 8.36 mm (0.329 in), and the cladding thickness is 0.57 mm (0.0225 in). The fuel assemblies consist of a 17×17 array of fuel rods. The center-to-center pitch of the rods is 12.598 mm (0.496 in). Thimble guide and Instrumentation rods are also included in the model and are assumed to have a similar size to the fuel rods. The 32 fuel assemblies are centered inside stainless steel channels that rest inside a honeycomb style basket made of aluminum plates of a 12.7 mm (0.5 in) thickness, neutron absorber BORAL plates of a 1.016 mm (0.04 in) thickness, and stainless steel plates with a 2.667 mm (0.105 in) thickness. The detail view region in Fig. 1 also shows a portion of the aluminum rails that are used as structural support for the honeycomb basket. The rails and basket are confined within an inner vessel used at the primary confinement barrier and made of SA-213 steel. Surrounding the inner vessel is a carbon steel gamma shield made of SA-266 steel with a thickness of 203.2 mm (8 in). A borated polyester neutron shield of 101.6 mm (4 in) thickness is encased in aluminum boxes and covers the gamma shield. The final layer of the cask is a steel shell of a thickness of 12.7 mm (0.5 in.) and acts as the final photon shield. The outer diameter of the cask is 2.483 m (~ 98 in.).

The model shown in Fig. 1 assumes that the gap between the basket and aluminum rails is uniform and equal to 4.78 mm. This model is called the "concentric" model. Two other models were created to investigate the effect of the basket leaning on one side or two sides of the cask. In these models, the size of the gap was changed by translating the basket and fuel regions. In the single-shift model, the fuel and basket regions are translated 4.78 mm along the positive *x*-axis, shown in Fig. 1, closing the vertical gaps on the right side of the basket and doubling them to 9.56

mm on the left side. The gaps on the top and bottom of the basket remain unchanged at 4.78 mm. In the double-shift model, the basket and fuel regions are translated 4.78 mm along the positive *x*-axis and 4.78 mm along the positive *y*-axis, closing the gaps on the right and top sides of the basket, and causing the gaps on the bottom and left sides to double to 9.56 mm.

In order to reduce the computational effort in modeling the full cask model for these three geometries (concentric, single-shift, double-shift), the symmetry of the cask is utilized. The concentric model (uniform gap) shown in Fig. 1 is symmetric along the *x* and *y*-axes, and the two diagonal axes at 45° and 135°, such that only one-eighth of the cask cross-section is enough to represent the full cask with symmetry boundary conditions on the two symmetry lines. The single-shift model is symmetric only about the *x*-axis, so one-half of the cask cross-section with symmetry boundary condition on the *x*-axis is modeled. The double shift model is symmetric only about the axis at 45^o. Similar to the single-shift model, only one-half of the cask cross-section with a symmetry boundary condition at the 45^o axis is modeled.

Boundary Conditions

Because the heat generation in real UNF assemblies is not uniform along their lengths, a peaking factor of 1.2 was applied to simulate the region of the assemblies with the highest heat generation rate [8]. For all simulations, conduction heat transfer through the solid and helium regions, and radiation heat transfer across all helium regions are modeled. Natural convection is not taken into account in the simulations because the buoyancy effect acts in the *z*-direction normal the plan of Fig. 1, which cannot be modeled using the 2D configurations considered in this work. The cask is assumed to dissipate heat to the ambient by both radiation and natural convection heat transfer. For radiation heat transfer, an ambient temperature of 46°C is employed with a cask outer surface emissivity of 0.9. For natural convection, a temperature-dependent heat transfer coefficient is applied on the outer surface of the cask. For the internal surfaces of the cask, an emissivity value of 0.3 was used for the all steel and aluminum surfaces, and a value of 0.8 was used for zircaloy surfaces. All the boundary conditions mentioned above were obtained from the Final Safety Analysis Report (FSAR) for the TN-32 [8].

To model the temperature-jump effect at low pressures, the Lin & Willis temperature-jump model (4) was used with a constant value of α = 0.3. This value of α corresponds to an average cask temperature of ~210°C. It should be mentioned here that α is temperature-dependent. Its value decreases as the temperature of the wall increases. However, ANSYS/Fluent does not allow for implementation of a temperature-dependent value of α.

Results and Discussion

Steady-state CFD simulations were performed in ANSYS/Fluent 19.1 using the three models (concentric, single-shift, and double-shift) for a heat generation rate of 1020 W/assembly in the UO_2 regions and different helium pressure conditions; (i) continuum condition with helium pressure of ~ 10^5 Pa and no temperature-jump boundary condition at the gas-solid interfaces, (ii) rarefied condition with helium pressures of 400 Pa and 100 Pa, and temperature-jump boundary conditions at the solid-gas interfaces with α = 0.3, and (iii) hard vacuum condition (P = 0 Pa) with only radiation heat transfer across the helium regions.

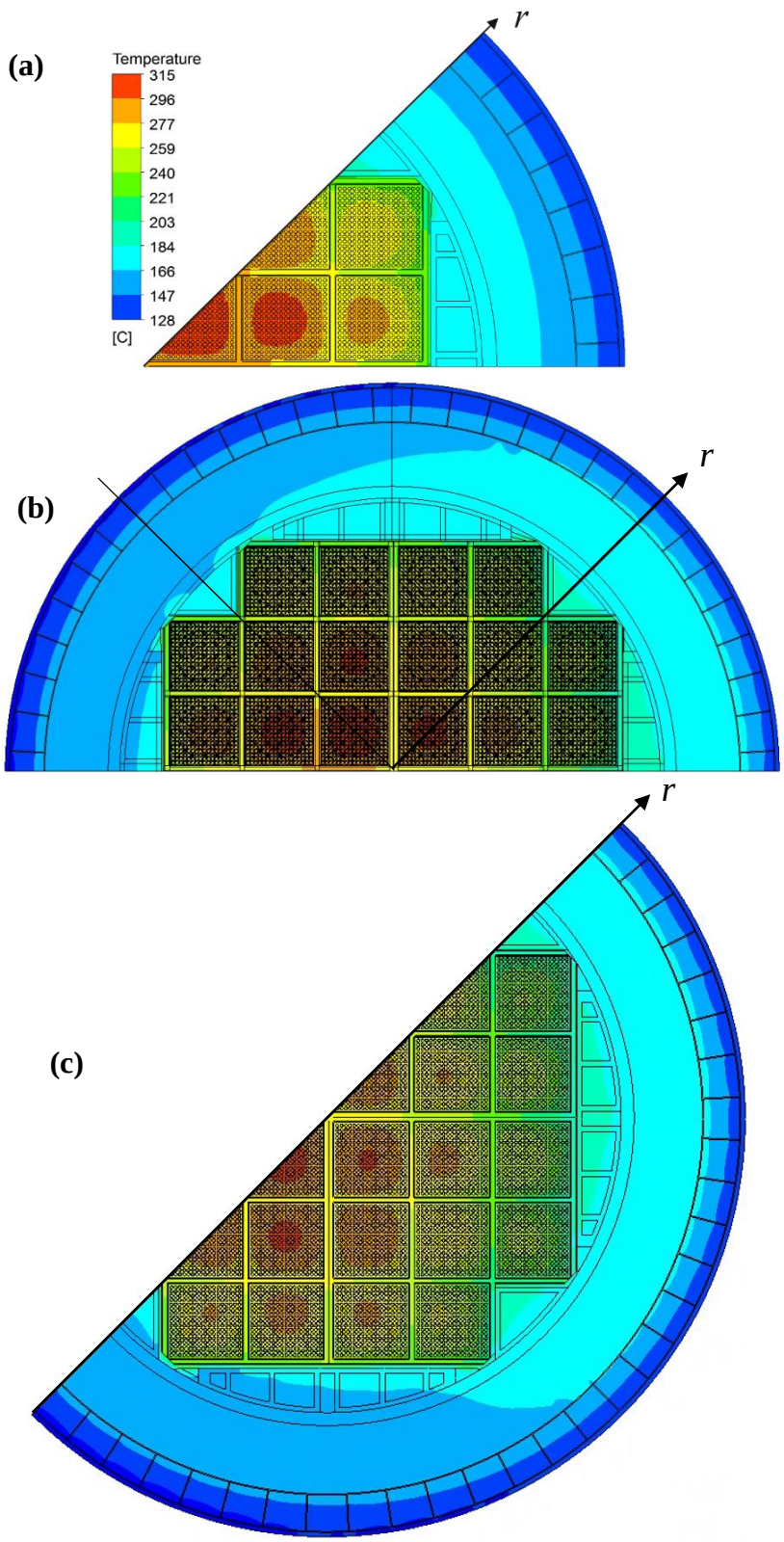

Figure 2: Temperature contour plots for (a) the concentric, (b) single-shift, and (c) double-shift models showing the temperature distribution within the cask for the continuum condition, $P \sim 10^5$Pa.

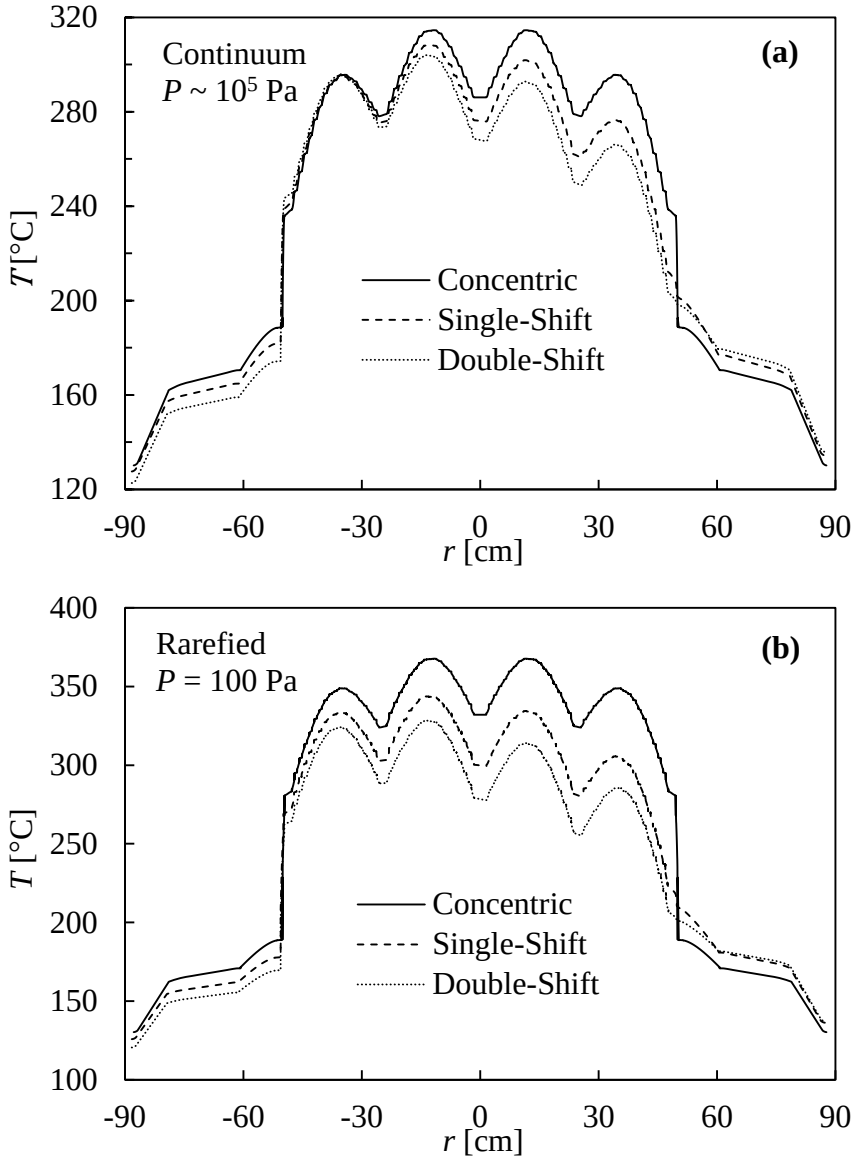

Figure 3: Temperature profile along the *r*-axes (shown in Fig. 2 for each of the three models) for a pressure of (a) $P \sim 10^5$ Pa (continuum), and (b) $P = 100$ Pa (rarefied).

Figure 2 shows the temperature contours for the continuum condition ($P \sim 10^5$ Pa) with no temperature-jump boundary condition for each of the three models. In the concentric model (Fig. 2a), there are local maximum cladding temperatures within each fuel assembly, but the global maximum is located near the center of the innermost fuel assembly. In the shifted models (Figs. 2b and 2c), the positions of the local maxima shift slightly away from the center of the model toward the sides with the largest gaps. This is because more heat leaves from the region of the basket with no gap. One can also notice that temperature distribution in the cask gamma shield is not uniform for the shifted models as opposed to the concentric model. This also due to the effect of the gap size. The peak cladding temperature obtained for the continuum condition is 315°C for the concentric model, 308°C for the single-shift model, and 304°C for the double-shift model, which are all below the radial hydride formation temperature limit, $T_{RH} = 400$°C.

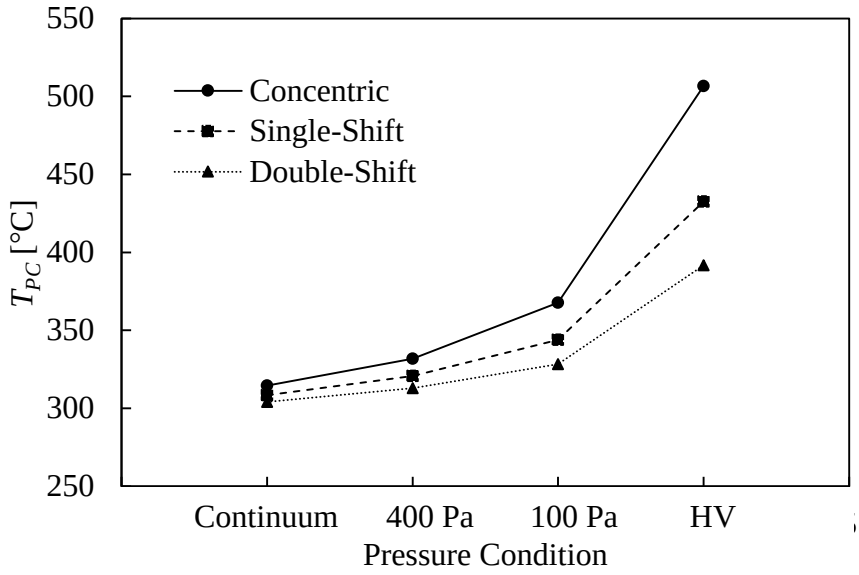

Figure 4: Peak cladding temperature in each of the models as functions of pressure condition.

Figure 3a shows the temperature profiles along the *r*-axes, shown in Fig. 2 for each model, for the continuum pressure condition. Because the concentric model is symmetric along the *r* and *x*-axes, the temperature profile was mirrored to cover the whole diameter of the cask. This figure shows that the profile of temperature for the concentric model exhibit maxima within the fuel assemblies and that there is a steep temperature gradient at around $r = 50$ or -50 cm, which are the locations of the gaps between the basket and rail. The temperature then gradually decreases to reach ~ 130°C at the outer surface. This figure also shows that the shifted models exhibit a non-symmetrical temperature profile along the *r*-axis because the heat is not transferred symmetrically. The temperature obtained at $r \sim -40$ cm is almost the same for all the models. However, as *r* increases, the temperature of the shifted models become smaller than the concentric model, with the double-shifted being the smallest, and this is up to $r = 50$ cm. For $r > 50$ cm, the opposite trend is observed, where the double-shifted model exhibits the highest temperature. This is because the gap between the basket and rail at $r = 50$ cm is closed, so more heat can pass through that side. It is worth noting that the concentric model is not always the hottest. At $r = -50$ cm, the double-shifted model is the hottest. This is due to the larger amount of insulation provided by the 9.56 mm gap in the double shifted model.

Figure 3b shows the temperature profiles along the *r*-axes shown in Fig. 2 for the rarefied condition, $P = 100$ Pa. These profiles are similar to the continuum profiles (Fig. 3a), but with a larger scale and more pronounced differences between the models. The effect of the temperature-jump in all the models caused their temperature to increase compared to the continuum condition. The temperature-jump is larger in the helium gaps between the basket and rails compared to the helium regions between the rods. For the concentric model, the temperature of the fuel assemblies is always larger than the shifted models, because of the large temperature-jumps at $r = 50$ or -50 cm. The same behavior is observed for the other rarefied $P = 400$ Pa and heard vacuum conditions.

Figure 4 shows the peak cladding temperature for each model as a function of the pressure condition. As the pressure decrease, the PCT increases for all the models. The concentric model

has the highest PCT for all conditions followed by the single-shifted then double shifted. The PCT difference between the models increases as the pressure decreases.

The maximum allowable heat generation rate, Q_{max}, that brings the cladding to the radial hydride formation temperature, T_{RH} = 400°C, for each model and each pressure condition is summarized in Table 1. The maximum allowable heat generation rate decreases with pressure in each model. The shifted models have a higher maximum allowable heat generation rate. The value of Q_{max} for the double shifted model is 1511 W/assembly, however for the concentric geometry, Q_{max} = 1439 W/assembly, which is 4.8% smaller. This reduction is even more pronounced with decreasing pressure. At P = 100 Pa and for concentric model, Q_{max} = 1156 W/assembly, which is 15.5 % smaller than that of the double-shift geometry, Q_{max} = 1368 W/assembly. The results presented above show that the concentric model is the most conservative of all the models.

Table 1: Maximum allowable heat generation rate per assembly that brings the fuel to T_{RH} = 400°C for each model (concentric, single-shift, and double-shift).

Model	Q_{max} [W/assembly]			
	Continuum	Rarefied		Hard Vacuum
	$P \sim 10^5$ Pa	P = 400 Pa	P = 100 Pa	
Concentric	1439	1335	1156	613
Single-Shift	1480	1403	1275	882
Double-Shift	1511	1456	1368	1059

Conclusion and Future Work

In this paper, the effect of the UNF cask fuel basket leaning on one or two sides of the cask, closing the gap on those sides, and enlarging them on the opposite sides, on the fuel assembly temperature is investigated in comparison with a concentric basket during the vacuum drying process. Steady-state simulations were conducted in ANSYS/Fluent on geometrically-accurate 2D models of a TN-32 nuclear fuel cask for continuum, rarefied, and hard vacuum pressure conditions.

The results showed that the concentric model exhibits the highest PCT for all pressure conditions. Therefore, it is the most conservative for simulations. The maximum allowable heat generation that brings the claddings temperature to the limit of 400°C is 1439 W/assembly for the concentric model, and it increases to 1480 and 1511 W/assembly for the single and double shifted models, respectively, in the continuum condition.

For future work, the concentric 2D model will be extruded in the third dimension to create a 3D half model that can be used to investigate the effects of an axially varying heat generation within the fuel regions. It will also be used to model forced gas dehydration. Additionally, not all assemblies within a cask necessarily have the same heat generation. The effect of different heat generation rates of the assemblies and their placement on the peak cladding temperature will also be investigated.

Acknowledgments

This work was supported by the U.S. Department of Energy Office of Nuclear Energy University Program under award number DE-NE0008713 and U.S. Nuclear Regulatory Commission under award number NRC-HQ-13-G-38-0027.

References

[1] U.S. Department of Energy, Office of Civilian Radioactive Waste Management, "Characteristics of Spent Nuclear Fuel, High-Level Waste, and Other Radioactive Wastes Which May Require Long- Term Isolation," DOE/RW-0184, (1987).

[2] D. COLMONT, P. ROBLIN, AND C. GUÉRIN, "Improved Thermal Modeling of a SNF Shipping Cask Drying," *International Conference on Mathematics, Computational Methods & Reactor Physics*, Saratoga Springs, New York, 3 - 7 May (2009).

[3] L. MILLER, D. BASU et *al*. "Overview of Vacuum Drying Methods and Factors Affecting the Quantity of Residual Water after Drying," U.S. Nuclear Regulatory Commission, NRC–02–07–006 (2013).

[4] W. LARGE and R. SINDELAR, "Review of Drying Methods for Spent Nuclear Fuel," *Westinghouse Savannah River Company*, report number WSRC-TR0075, Savannah River Site, Aiken, SC (1997).

[5] U.S. Nuclear Regulatory Commission, "Cladding Considerations for the Transportation and Storage of Spent Fuel," ISG-11 R3, Interim Staff Guidance Report of the Spent Fuel Project (2003).

[6] J. T. LIN and D. R. WILLIS, "Kinetic Theory Analysis of Temperature Jump in a Polyatomic Gas," Phys. Fluids, vol. 15, p. 31 (1972).

[7] M. HIGLEY, M. HADJ-NACER, AND M. GREINER, "Temperature Prediction of a TN-32 Used Nuclear Fuel Canister Subjected to Vacuum Drying Conditions," Pressure Vessels & Piping Division Conference, Prague Czech Republic, 15-20 July (2018).

[8] Transnuclear, Inc. "TN-32 Final Safety Analysis Report (FSAR), Revision 2" Nuclear Regulatory Commission Report # ML16097A219 (2002).

[9] Transnuclear, Inc. "TN-32 Dry Storage Cask System: Safety Evaluation Report" Nuclear Regulatory Commission Report # ML003696918.

[10] B. Hanson, "High Burnup Spent Fuel Data Project & Thermal Modeling and Analysis," *Nuclear Waste Technical Review Board Meeting*, Albuquerque, New Mexico, 24 October (2018).

[11] S.A. Schaaf and P.L. Chambre, *Flow of Rarefied Gases*, Princeton University Press, New Jersey (1961).

[12] S. Song and M. Yovanovich, "Correlation of Thermal Accommodation Coefficient for Engineering' Surfaces," (1987).

[13] L. Thomas and S. Loyalka, "Determination of Thermal Accommodation Coefficients of Helium, Argon, and Xenon on a Surface of Zircaloy-2 at about 25oC," *Nuclear Technology*, 57, 213, (1982).